

Origin of ferroelectricity in the multiferroic barium fluorides BaMF_4

Claude Ederer and Nicola A. Spaldin

Materials Department, University of California, Santa Barbara, CA 93106, U.S.A.*

(Dated: September 26, 2018)

We present a first principles study of the series of multiferroic barium fluorides with the composition BaMF_4 , where M is Mn, Fe, Co, or Ni. We discuss trends in the structural, electronic, and magnetic properties, and we show that the ferroelectricity in these systems results from the “freezing in” of a single unstable polar phonon mode. In contrast to the case of the standard perovskite ferroelectrics, this structural distortion is not accompanied by charge transfer between cations and anions. Thus, the ferroelectric instability in the multiferroic barium fluorides arises solely due to size effects and the special geometrical constraints of the underlying crystal structure.

I. INTRODUCTION

Magnetoelectric multiferroics are currently attracting much attention.^{1,2} These materials, which exhibit magnetic and dielectric order in the same phase, can give rise to interesting coupling effects between the two ferroic order parameters, with great potential for technological applications. Currently, the main research effort in multiferroics is directed towards Bi-containing perovskites such as BiFeO_3 or BiMnO_3 ,^{3,4,5} and towards both hexagonal and orthorhombic rare-earth manganites such as HoMnO_3 and TbMnO_3 .^{6,7} In the present article we revisit another class of magnetic ferroelectrics: the barium fluorides BaMF_4 , where M is Mn, Fe, Co, or Ni. This series of compounds attracted considerable interest from the late 1960s until the early 1980s (see Ref. 8 and references therein) but so far has not received much attention during the recent revival of multiferroic materials. We hope that our work will inspire further research in this interesting class of multiferroic materials, with the goal of exploring a broader range of non-oxide-based materials as candidates for magnetoelectric device applications.

The barium fluorides BaMF_4 , $M = \text{Mn, Fe, Co, Ni, Zn, and Mg}$, form an isostructural family of compounds with the polar space group $Cmc2_1$ (Refs. 9,10).⁶⁰ The corresponding crystal structure is shown in Fig. 1a. In this base-centered orthorhombic structure the transition metal cations are octahedrally surrounded by fluorine anions. Four of the six corners of the fluorine octahedra are shared with adjacent octahedra to form puckered sheets perpendicular to the orthorhombic b axis. These sheets of octahedra are separated by similar sheets of Ba cations. The structure is polar along the c direction, and ferroelectric switching has been demonstrated for $M = \text{Co, Ni, Zn, and Mg}$, but not for $M = \text{Mn and Fe}$.¹⁰ The dielectric constants ϵ_c show an increase with temperature that is characteristic for a ferroelectric phase transition, but all crystals melt before a transition into the paraelectric phase occurs. The melting temperatures range between 720–965 °C; the Curie-Weiss temperatures can be extrapolated from the temperature dependence of the dielectric constants and range between 810–1320 °C.¹¹ In BaMnF_4 an additional structural phase transition occurs at ~ 255 K.¹² The resulting low-temperature structure is

incommensurate along the c axis.¹³ To facilitate a systematic comparison between the different BaMF_4 systems we do not consider this low temperature structure of BaMnF_4 in the present study and instead use perfect $Cmc2_1$ symmetry for all systems.

In addition to the polar distortion, the systems with $M = \text{Mn, Fe, Co, and Ni}$ exhibit antiferromagnetic ordering below $T_N \approx 50 - 120$ °C.¹⁴ These materials therefore exhibit multiferroic behavior, which is the motivation for the present investigation.

Here we present a comprehensive computational study of the structural, electronic, magnetic, and ferroelectric properties of BaMF_4 , with $M = \text{Mn, Fe, Co, and Ni}$, using first principles electronic structure calculations. The goal is to elucidate the origin of ferroelectricity in these materials, and to understand trends, such as why the systems with $M = \text{Mn and Fe}$ do not exhibit ferroelectric switching. The origin of ferroelectricity is of fundamental interest, since BaMF_4 does not contain any ions, which are usually considered to be “ferroelectrically active”, such as empty d shell cations or lone pair-active cations (e.g. Bi^{3+} , Pb^{2+}).^{15,16} We show that the ferroelectricity in these systems is due to the softening of a single polar phonon mode, which involves both rotational motions of the fluorine octahedra and polar displacements of the Ba cations. The instability is caused solely by size effects and geometrical constraints; no charge transfer between anions and cations occurs as a result of the structural distortion. The BaMF_4 multiferroics therefore represent an example of proper “geometric ferroelectricity”, a mechanism that has been proposed as a possible way to incorporate both magnetism and ferroelectricity in the same system.^{17,18} Furthermore, our work represents the first *ab initio* study of a non-oxide multiferroic system, and we provide evidence that the LSDA+ U method results in a good description of the electronic structure of these materials.

This paper is organized as follows. We first describe the methods we use in our calculations, together with some technical details. We then present the results of our calculations for the structural, electronic, and magnetic properties of all systems. Finally, we focus on the ferroelectric properties and analyze the mechanism underlying the polar structural distortions in these systems. We end with a discussion and summary.

II. COMPUTATIONAL METHOD

All calculations in this work are performed using the projector augmented-wave method,¹⁹ implemented in the VIENNA AB-INITIO SIMULATION PACKAGE (VASP).^{20,21} For the treatment of exchange and correlation we use both the local spin-density approximation (LSDA)²² and the LSDA+ U method in the formulation of Dudarev *et al.*,²³ which is equivalent to the standard form of Anisimov *et al.*,²⁴ with the intra-atomic exchange parameter J set to zero (see Ref. 25). For the Hubbard parameter $U_{\text{eff}} = U - J$ of the transition metal d states we use a typical value of 4 eV, and we test the sensitivity of our results with respect to the precise value of U_{eff} where necessary (see also section III B).

To obtain structural parameters we relax all ions until the Hellman-Feynman forces are less than 0.01 eV/Å, and we adjust the lattice vectors such that all components of the stress tensor are smaller than 1 kbar. During the relaxations, except where otherwise noted, we impose the experimentally observed antiferromagnetic order (see Sec. III C), which doubles the size of the unit cell and reduces the space group symmetry to monoclinic. However, no monoclinic distortion has been found experimentally, and in our calculations the corresponding effect, if present, is too small to be resolved unambiguously. We therefore neglect a possible monoclinic distortion and restrict the lattice vectors to the orthorhombic symmetry. For test purposes, we also perform relaxations for different magnetic structures, e.g. ferromagnetic ordering.

To obtain local densities of states we define spheres around the ions with radius 1.0 Å for the M cations and 0.9 Å for the fluorine anions. We use a $4 \times 4 \times 3$ Monkhorst-Pack k-point mesh (divisions with respect to the base-centered orthorhombic lattice vectors of the nonmagnetic unit cell) and a Gaussian smearing of 0.1 eV for Brillouin zone integrations. The plane-wave energy cutoff is set to 550 eV for relaxations and to 450 eV for all other calculations. To calculate the spontaneous polarization we use the Berry-phase approach^{26,27,28} and integrate over 8 homogeneously distributed k-point strings parallel to the reciprocal c direction, each string containing 8 k-points. For the calculation of the force-constant matrix we displace all the ions by 0.005 Å, corresponding to symmetry-adapted modes. To exclude eventual nonlinearities in the forces we repeat the calculation with displacements of 0.01 Å, which leads to identical values for the force constant matrix.

III. RESULTS AND DISCUSSION

A. Structural properties

Table I shows the structural parameters for all systems obtained here by using both LSDA and LSDA+ U with $U_{\text{eff}} = 4$ eV, together with experimental data. The overall agreement between calculated and experimental values is

very good. The use of the LSDA leads to a typical underestimation of the lattice parameters between 1–4% whereas the internal structural parameters are very close to the experimental values. The LSDA+ U method leads to a slightly larger equilibrium volume compared to the pure LSDA and therefore improves the agreement with experiment. This is very similar to what has been reported previously for several magnetic oxides.^{4,33,34}

The calculated structural parameters shown in Table I are calculated for the experimentally observed antiferromagnetic order (see Sec. III C). If a different magnetic structure is imposed during the relaxation (results not shown here), we notice small, but distinct, structural changes. For example, relaxation of BaNiF₄ in a ferromagnetic configuration leads to a 0.8% increase in the lattice parameter b and up to 7% change in the Wyckoff positions of those fluorine ions that mediate the magnetic superexchange interactions in the M -F- M bonds. This indicates a certain degree of spin-lattice coupling in these systems which can give rise to phenomena such as spin-phonon coupling³⁵ and magneto-capacitance.³⁶

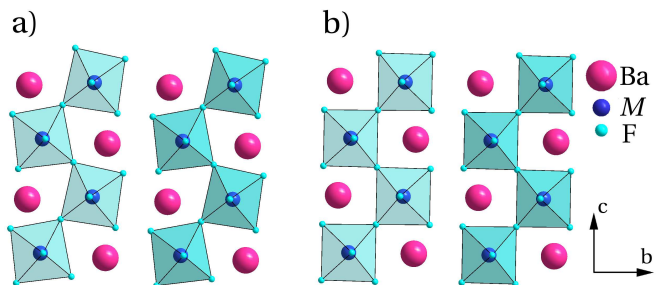


FIG. 1: (Color online) a) Projection of the BaMF₄ structure along the a axis. The M cations are octahedrally surrounded by fluorine anions, which form puckered sheets perpendicular to the b axis, separated by similar sheets of Ba cations. Adjacent sheets are shifted relative to each other by half a lattice constant along the a direction. b) Corresponding centrosymmetric prototype structure.

We also performed structural relaxations for all systems within the corresponding centrosymmetric prototype structure with space group symmetry $Cmcm$ (see Ref. 29 and Fig. 1b), which can be obtained from the ground state structure by imposing an additional mirror symmetry perpendicular to the c axis. It has been suggested that the M -F(1)- M distance in this centrosymmetric $Cmcm$ structure is too small to accommodate two M -F bonds, causing the structural instability in the BaMF₄ systems.²⁹ Here, F(1) is the fluorine anion connecting neighboring octahedra along the c direction. The M -F(1)- M segment thus “bends” outward in order to increase the M -F(1) bond length, leading to the observed collective distortion of the octahedral network. This distortion can be understood as collective alternate rotations of the fluorine octahedra around their respective centers with the rotation axis parallel to the a direction, accompanied by displacements of the Ba cations paral-

TABLE I: Structural parameters for $Cmc2_1$ $BaMF_4$, $M=Mn, Fe, Co, Ni$, obtained using the LSDA and the LSDA+ U method with $U_{\text{eff}}=4$ eV together with experimental data. a, b, c are the usual orthorhombic lattice constants, V is the corresponding volume, d represents the atomic displacements compared to the $Cmcm$ centrosymmetric reference structure. All atomic positions correspond to Wyckoff-positions $4a: (0,y,z)$.

| | Mn | | | Fe | | | Co | | | Ni | | | |
|-----------------------|---------|-----------------------|------------|--------|-----------------------|------------|--------|-----------------------|------------|--------|-----------------------|------------|--------|
| | LSDA | $U_{\text{eff}}=4$ eV | Expt. [29] | LSDA | $U_{\text{eff}}=4$ eV | Expt. [30] | LSDA | $U_{\text{eff}}=4$ eV | Expt. [31] | LSDA | $U_{\text{eff}}=4$ eV | Expt. [32] | |
| a [Å] | 4.18 | 4.18 | 4.22 | 4.20 | 4.21 | 4.24 | 4.15 | 4.10 | 4.21 | 4.08 | 4.08 | 4.14 | |
| b [Å] | 14.58 | 14.70 | 15.10 | 14.30 | 14.52 | 14.86 | 14.05 | 14.08 | 14.63 | 13.85 | 13.95 | 14.43 | |
| c [Å] | 5.81 | 5.85 | 5.98 | 5.63 | 5.59 | 5.83 | 5.65 | 5.78 | 5.85 | 5.65 | 5.67 | 5.78 | |
| V [Å ³] | 354.4 | 359.5 | 381.4 | 338.0 | 341.7 | 367.2 | 328.9 | 333.4 | 360.3 | 319.4 | 323.0 | 345.1 | |
| Ba | y | 0.152 | 0.154 | 0.156 | 0.145 | 0.148 | 0.151 | 0.142 | 0.143 | 0.148 | 0.139 | 0.141 | 0.146 |
| | z | -0.043 | -0.047 | -0.047 | -0.035 | -0.034 | -0.041 | -0.032 | -0.040 | -0.039 | -0.026 | -0.031 | -0.036 |
| Ni | y | 0.414 | 0.414 | 0.416 | 0.410 | 0.411 | 0.414 | 0.409 | 0.410 | 0.413 | 0.408 | 0.409 | 0.412 |
| | z | 0.000 | 0.000 | 0.000 | 0.000 | 0.000 | 0.000 | 0.000 | 0.000 | 0.000 | 0.000 | 0.000 | 0.000 |
| F(1) | y | -0.464 | -0.462 | -0.465 | -0.471 | -0.468 | -0.469 | -0.477 | -0.474 | -0.472 | -0.483 | -0.479 | -0.475 |
| | z | -0.158 | -0.157 | -0.163 | -0.171 | -0.157 | -0.166 | -0.191 | -0.191 | -0.179 | -0.210 | -0.200 | -0.187 |
| F(2) | y | 0.298 | 0.298 | 0.298 | 0.299 | 0.300 | 0.301 | 0.300 | 0.299 | 0.302 | 0.302 | 0.301 | 0.303 |
| | z | 0.205 | 0.202 | 0.196 | 0.212 | 0.208 | 0.198 | 0.213 | 0.204 | 0.198 | 0.217 | 0.211 | 0.202 |
| F(3) | y | -0.327 | -0.329 | -0.336 | -0.324 | -0.323 | -0.331 | -0.325 | -0.329 | -0.334 | -0.322 | -0.325 | -0.333 |
| | z | 0.224 | 0.225 | 0.225 | 0.229 | 0.230 | 0.223 | 0.231 | 0.227 | 0.227 | 0.236 | 0.234 | 0.231 |
| F(4) | y | -0.077 | -0.079 | -0.078 | -0.078 | -0.080 | -0.080 | -0.080 | -0.076 | -0.079 | -0.082 | -0.081 | -0.081 |
| | z | 0.011 | 0.018 | 0.016 | -0.001 | -0.001 | 0.006 | -0.001 | 0.007 | 0.011 | -0.002 | 0.000 | 0.007 |
| Ba | d [Å] | 0.256 | 0.276 | — | 0.203 | 0.202 | — | 0.190 | 0.238 | — | 0.152 | 0.181 | — |
| F(1) | d [Å] | 0.751 | 0.775 | — | 0.607 | 0.695 | — | 0.467 | 0.501 | — | 0.329 | 0.409 | — |

l to the polar c axis. Table I shows the magnitude of the displacements d of both the Ba and F(1) ions leading from the centrosymmetric reference structure to the polar ground state structure. From these displacements it can be seen that the structural distortion increases over the series from $M = Ni$ to $M = Mn$, which is also consistent with the experimental observations, and has been explained by a decrease in the ratio between the M - M distance and the minimum M - F bond length when M is changed from Ni to Mn.²⁹

B. Electronic structure

The calculated total densities of states as well as the partial densities of the fluorine p and transition metal d states for all systems are shown in Figure 2. For $M = Mn$ and Ni, even the use of the LSDA leads to an insulating solution. In the case of the Ni system the gap is small and is due to the crystal field splitting of the localized d states, whereas in the Mn system the gap is larger and is produced mainly by the strong exchange splitting between the two spin channels. The Fe and Co systems are metallic in LSDA, as expected for the d^6 and d^7 electron configurations of the Fe^{2+} and Co^{2+} ions within the predominantly cubic crystal field. The very small bandwidth of the transition metal d states indicates an instability towards the formation of a Mott-Hubbard gap, and indeed the use of the LSDA+ U method with $U_{\text{eff}} = 4$ eV leads to the formation of a large gap of about 2–3 eV for $M = Fe$ and Co, and to a substantial increase in the width of the gap for the Mn and Ni systems. In all cases

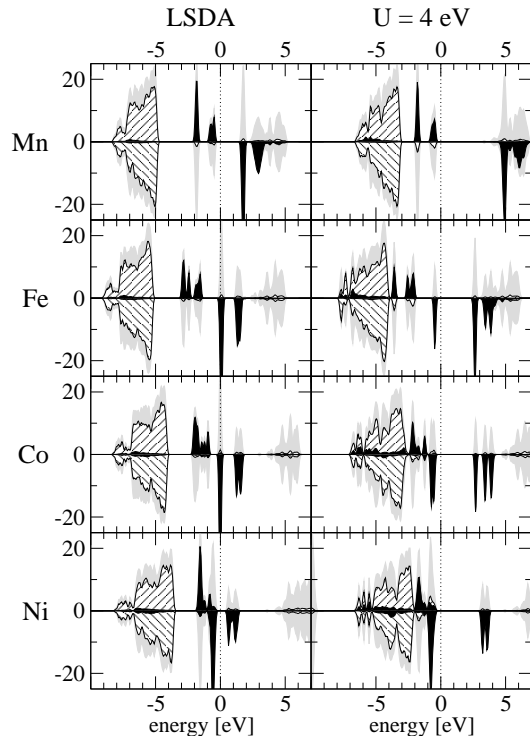


FIG. 2: Total densities of states (gray shaded), partial fluorine p (shaded with thin diagonal lines) and transition metal d (black shaded) states (in states/eV), calculated within the LSDA (left panel) and by using $U_{\text{eff}} = 4$ eV (right panel) for all $BaMF_4$ systems ($M = Mn, Fe, Co, Ni$ from top to bottom). Minority spin states are shown with negative sign. Zero energy corresponds to the Fermi level (metallic systems) or the highest occupied state (insulating systems).

the gap is between occupied and unoccupied d states of the transition metal ion.

These results indicate that the use of the LSDA is inadequate for the BaMF_4 systems, whereas the LSDA+ U method with an appropriate U value leads to a good description of the electronic structure. In this work, except where otherwise noted, we use $U_{\text{eff}}=4\text{eV}$, which is a typical value for transition metal cations in oxide materials.^{37,38,39} Since the overall features of the transition metal d states in the present fluorides are very similar to the oxide case, we expect that the same value of U is also appropriate for these systems. We point out that a variation of U within reasonable limits alters the electronic structure only qualitatively. Nevertheless, for quantities that are expected to depend critically on U , we always consider the explicit U dependence.

It can be seen from Fig. 2 that all transition metal cations are in a high-spin configuration, where the local majority spin states are fully occupied, and the minority spin states are filled with 0, 1, 2, 3 electrons for $M = \text{Mn, Fe, Co, Ni}$, respectively. In the case of the LSDA, the transition metal d states are energetically well separated from the fluorine p states, leading to only negligible hybridization between the two sets of states. The use of LSDA+ U lowers the energy of the filled transition metal d states, leading to energetic overlap of these states with the fluorine p levels and a certain degree of hybridization, which is most notable for $M = \text{Ni}$. This increase in hybridization with increasing U could be an artifact of the LSDA+ U method, which only corrects the transition metal d states while leaving the fluorine p states unchanged.

The densities of states for the centrosymmetric $Cmcm$ structures (not shown here) are indistinguishable from those calculated for the ground state structures (both in LSDA and LSDA+ U). This indicates that the structural distortions in these systems do not lead to a significant change in covalent bonding, in contrast to the case of the ferroelectric perovskites, where the structural distortions lead to strong rehybridization between filled anion p and empty cation states.^{40,41} We will further analyze the ferroelectric instability of the BaMF_4 systems in Sec. III D.

C. Magnetic properties

The experimentally observed magnetic structure is shown in Fig. 3.⁴² The magnetic M cations form quasi-two-dimensional puckered rectangular grids “parallel” to the a - c planes. Within each rectangular grid the magnetic moments of nearest neighbors are aligned antiparallel to each other. The coupling between adjacent grids effectively cancels, so that the magnetic order along the b direction is determined by the weak coupling between the next nearest neighbor planes that are $\sim 14 \text{ \AA}$ apart. This can lead to two different magnetic phases, in which the coupling along the b direction is either parallel (phase B) or antiparallel (phase A). Both phases have been ob-

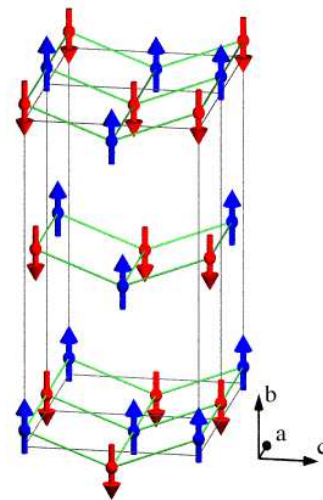


FIG. 3: (Color online) Magnetic structure of BaMF_4 , $M = \text{Mn, Fe, Ni}$ (only magnetic ions are shown). For $M = \text{Co}$ (phase A) the magnetic moments are oriented parallel to the c axis, but the relative orientations of the moments are the same. Gray lines outline the conventional orthorhombic unit cell; the puckered rectangular grids are shown in green.

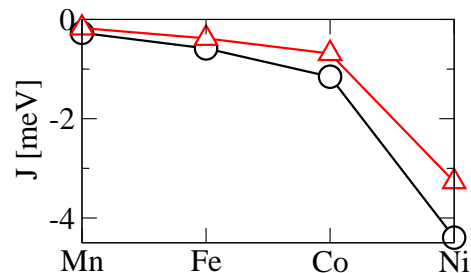


FIG. 4: Heisenberg nearest neighbor exchange coupling constants J_a (circles) and J_c (triangles).

served for BaCoF_4 ,⁴³ and since the energy difference between these two phases is very small, it is generally assumed that extrinsic effects such as defects etc. can lead to the preferred appearance of one or the other phase. In our calculations we only consider phase A where the coupling between second nearest neighbor planes along the b direction is antiparallel. In all systems except BaCoF_4 the magnetic moments are oriented parallel to the b axis, whereas in BaCoF_4 the magnetic moments are oriented parallel to the c axis (in both phase A and phase B).⁴³

The magnetic structure of BaMnF_4 exhibits two distinct variations of the structure described in the previous paragraph and shown in Fig. 3: first, the antiferromagnetic axis is rotated by 9° from the b towards the a direction,⁴⁴ and in addition all magnetic moments are slightly canted towards the c direction by about 0.1° , resulting in a very small magnetization.⁴⁵

We do not attempt to reconstruct the full magnetic structure of all BaMF_4 systems from first principles, but to check if the LSDA+ U treatment of the electron-

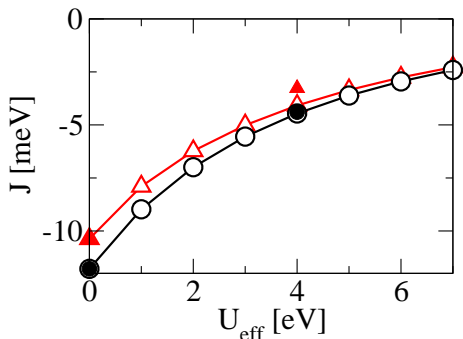


FIG. 5: Heisenberg coupling constants for BaNiF_4 as a function of U_{eff} (J_a : circles, J_c : triangles). Open symbols correspond to calculations done with structural parameters obtained within LSDA. Filled symbols correspond to fully relaxed calculations.

electron interaction leads to a correct description of the magnetic properties of the multiferroic barium fluorides, we determine the nearest neighbor magnetic coupling constants for all systems. To do this, we first calculate the energy differences corresponding to different magnetic configurations of the four spins in the unit cell. We then map the calculated energies on a simple Heisenberg model, where we write the magnetic interaction as $E_{ij} = -2J_{ij}s_i \cdot s_j$ (s_i is the spin of cation i ; J_{ij} is the coupling constant between ions i and j) and consider only nearest neighbor interactions. Within our sign convention a negative J_{ij} corresponds to antiferromagnetic coupling.

Fig. 4 shows the calculated Heisenberg coupling constants J_a and J_c corresponding to pairs of nearest neighbor spins along the a and c direction, respectively, for $M = \text{Mn, Fe, Co, and Ni}$. All nearest neighbor couplings are antiferromagnetic, in agreement with the experimentally observed magnetic structure. The coupling becomes stronger from $M = \text{Mn}$ to Ni , which is a consequence of the successive filling of the t_{2g} states (see Ref. 46). In addition, the stronger hybridization between the transition metal d and fluorine p states in the case of the Ni system further increases the strength of the superexchange interaction, leading to particularly strong antiferromagnetic nearest neighbor coupling in BaNiF_4 .

For BaMnF_4 we obtain the exchange coupling constants $J_a = -0.270 \text{ meV}$ and $J_c = -0.173 \text{ meV}$ (using $U_{\text{eff}} = 4 \text{ eV}$). This compares extremely well with experimental values that have been extracted from the measured spin-wave dispersion: $J_a = -0.282 \text{ meV}$ and $J_c = -0.197 \text{ meV}$ (Ref. 13). This very good agreement might be to some extent fortuitous, but can also be regarded as strong indication that the value of U_{eff} indeed provides a good description of the electronic structure, since the magnetic superexchange coupling depends very strongly on U (see Fig. 5 and the following paragraph).

From the theory of superexchange it follows that the corresponding coupling constant is proportional to $1/U$.⁴⁶ One therefore expects a rather strong influence of

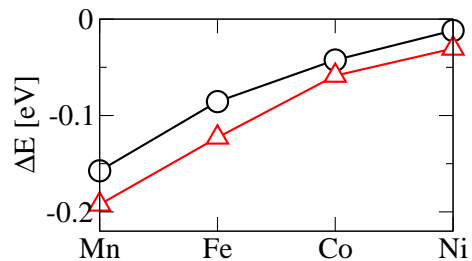


FIG. 6: Energy differences ΔE per formula unit between the ferroelectric and the centrosymmetric prototype structures, calculated within the LSDA (circles) and by using $U_{\text{eff}}=4 \text{ eV}$ (triangle).

the Hubbard parameter on the strength of the magnetic coupling, if this coupling is mediated mainly by the superexchange interaction. Indeed, strong U dependence of the magnetic coupling constants has been found for various oxides.^{47,48,49} Fig. 5 shows the variation of J_a and J_c in BaNiF_4 with the Hubbard parameter U_{eff} used in the LSDA+ U treatment of the electron-electron interaction. To see the pure electronic effect on the coupling constant, the structural parameters are kept fixed to their values obtained by the LSDA relaxation. It is apparent that the coupling strength significantly decreases with increasing U_{eff} , although the variation does not show an exact $1/U$ dependence. This is due to the fact that a variation of U in the bandstructure calculation also changes the overlap of the wave-functions and therefore the transfer integrals, which are considered as constant in the theory of superexchange.

The values corresponding to the relaxed structural parameters for $U_{\text{eff}} = 4 \text{ eV}$ are also shown in Fig. 5. It can be seen that there is only a negligible change of J_a , whereas J_c is reduced by 20% due to the slightly different structure. This is due to the fact that the bond lengths and angles for the $\text{Ni-F}(4)\text{-Ni}$ bond, which determines J_a , are nearly identical in LSDA and LSDA+ U , whereas the $\text{Ni-F}(1)\text{-Ni}$ bond angle, which determines J_c , is reduced from 160.5° (LSDA) to 155.8° ($U_{\text{eff}} = 4 \text{ eV}$). The $\text{Ni-F}(1)$ distance increases slightly from 1.94 \AA (LSDA) to 1.96 \AA ($U_{\text{eff}} = 4 \text{ eV}$).

In addition, if spin-orbit coupling is taken into account, there are small deviations from the collinear antiferromagnetic structure,⁵⁰ which are due to the antisymmetric exchange or Dzyaloshinskii-Moriya interaction.⁵¹ This small canting does not influence the structural and ferroelectric properties studied in the present paper, and we therefore neglect all effects due to spin-orbit coupling here.

D. Ferroelectric properties

Fig. 6 shows the energy differences per formula unit between the polar ground-state $Cmc2_1$ structures and the corresponding centrosymmetric $Cmcm$ structures, calcu-

TABLE II: Spontaneous polarizations (in $\mu\text{C}/\text{cm}^2$) calculated with an ionic model using formal charges and by using the Berry-phase approach ($U_{\text{eff}} = 4 \text{ eV}$), together with available experimental data.

| | ionic model | Berry phase | Exp. [10] |
|----|-------------|-------------|-----------|
| Mn | 13.68 | 13.60 | — |
| Fe | 10.34 | 10.88 | — |
| Co | 8.57 | 9.02 | 8.0 |
| Ni | 6.34 | 6.79 | 6.7 |

lated within the LSDA and by using LSDA+ U with $U_{\text{eff}} = 4 \text{ eV}$. The latter results in slightly larger energy differences, but the overall trend is similar in the two cases. The energy difference is largest for $M = \text{Mn}$ and smallest for $M = \text{Ni}$, consistent with the trend in the magnitude of the structural distortions (see Sec. III A). The fact that no ferroelectric switching could be observed for BaMF_4 with $M = \text{Mn}$ and Fe ¹⁰ has been explained by suggesting a rather high energy for the intermediate centrosymmetric state in these two systems, which results from the different equilibrium bond lengths compared to the systems with $M = \text{Co}$, Ni , Zn , and Mg .²⁹ This energy barrier is exactly the energy difference shown in Fig. 6. The values for $M = \text{Ni}$ and $M = \text{Mn}$ are comparable with the corresponding energy differences between ferroelectric and centrosymmetric prototype structures in the perovskite ferroelectrics BaTiO_3 ($\approx 18 \text{ meV/f.u.}$) and PbTiO_3 ($\approx 200 \text{ meV/f.u.}$), respectively.⁴⁰ Although it is not likely that ferroelectric switching actually takes place through the centrosymmetric reference structure, this energy difference can be viewed as an upper limit for the switching barrier. It is apparent that a classification of the Co and Ni systems as ferroelectric and the Mn and Fe systems as merely pyroelectric is probably not very instructive, since there is only a gradual quantitative difference between these systems. It seems feasible that ferroelectric switching could be achieved at least for the Fe system if highly resistive samples were available that could sustain higher electric fields.

From the displacements of the ions between the centrosymmetric prototype and the polar ground state structure it is possible to calculate an estimate of the spontaneous polarization using the formal charges of the ions (2+ for the cations and 1- for the fluorine anions). Table II lists the polarization values calculated from such an ionic model together with the corresponding values obtained by *ab initio* calculation using the Berry-phase theory of electric polarization.^{26,27,28} The good agreement between the Berry-phase result and the ionic model indicates that the Born effective charges⁵² are very close to their formal values for all systems. This is consistent with the lack of significant changes in the electronic densities of states between the centrosymmetric and distorted structures as described in Sec. III B. Thus, no significant charge transfer occurs as a result of the polar

TABLE III: TO phonon frequencies ω of A_g and B_{1u} symmetry for BaNiF_4 . x gives the contribution of the corresponding mode to the ground state distortion.

| A_g | ω [cm^{-1}] | 96 | 168 | 256 | 300 | 502 | |
|----------|-------------------------------|-------------|-----|-----|-----|-----|-----|
| | x [%] | 7 | 3 | 1 | 0 | 0 | |
| B_{1u} | ω [cm^{-1}] | $i\cdot 58$ | 151 | 212 | 256 | 397 | 541 |
| | x [%] | 87 | 1 | 0 | 0 | 0 | 0 |

distortion. This again indicates that the ferroelectricity in these systems is of different origin than in the prototypical perovskite ferroelectrics where charge transfer between the transition metal d and the anion p states is crucial for stabilizing the ferroelectric state.⁴⁰

To obtain further insight into the ferroelectric instability of these systems, we calculate the TO phonon frequencies of the centrosymmetric structure for BaNiF_4 . Since we are only interested in the phonon modes that are compatible with the observed ground state symmetry (only these modes can give rise to the corresponding structural distortions), we transform the dynamical matrix to block-diagonal form using symmetry-adapted modes, and diagonalize only the blocks corresponding to the irreducible representations A_g and B_{1u} of space group $Cmcm$. The nonpolar A_g phonons do not change the symmetry of the system, whereas the infrared active B_{1u} modes reduce the symmetry to the ground state $Cmc2_1$ space group. There are 5 A_g and 7 B_{1u} modes. The calculated phonon frequencies are listed in Table III. One of the 7 B_{1u} modes corresponds to an acoustic mode with zero frequency at the Γ point and is not included in Table III.

We find that there is one unstable B_{1u} mode with $\omega = i\cdot 58 \text{ cm}^{-1}$. If we decompose the structural distortion leading from the centrosymmetric reference structure to the relaxed ground state structure into contributions from the different phonon modes, we see that the unstable B_{1u} mode is responsible for about 87% of the final distortion. This indicates that the ferroelectricity in the barium fluorides originates from the softening of a single polar phonon mode which “freezes in” to form the ferroelectric ground state of the system. In contrast to the well-known case of perovskite ferroelectrics such as BaTiO_3 or PbTiO_3 no charge transfer between anions and cations occurs as a result of the displacements, which would lead to anomalous values of the Born effective charges, but instead the structural distortion in the BaMF_4 systems is driven purely by size effects, which, together with the special geometric connectivity realized in these compounds, leads to an inversion symmetry breaking and the appearance of a spontaneous electric polarization.

IV. DISCUSSION AND SUMMARY

It is well known that size-effects can drive structural distortions. For example in the perovskite system the relative ionic radii of the A and B cations determine the stability towards tilts of the anion octahedra.⁵³

The idea that ionic polarizability is, in general, not necessary for achieving ferroelectricity was already formulated in Ref. 54, when a ferroelectric ground state was predicted for perovskite-like NaCaF_3 on the basis of atomistic simulations using Gordon-Kim pair-potentials.⁵⁵ Since the possibility of covalent bond formation is excluded within this method, it became clear that a different mechanism is driving the ferroelectric distortion in NaCaF_3 . Although the underlying mechanism was not investigated any further, it was assumed that ionic polarizability would significantly enhance the ferroelectricity in NaCaF_3 . The present study shows that this does not necessarily have to be the case. Ferroelectricity was also predicted recently for a variety of perovskite-like fluorides, such as LiMgF_3 , LiNiF_3 , and NaCdF_3 .^{56,57} It is reasonable to assume that the ferroelectricity in all these fluoride systems is driven purely by size effects and that no charge transfer between anions and cations occurs.

It was pointed out recently that such a mechanism for ferroelectricity is compatible with the simultaneous occurrence of magnetic ordering.¹⁷ Using first principles electronic structure calculations, the hexagonal multiferroic YMnO_3 was identified as an example for such a scenario. In this material no charge transfer occurs as a result of the structural distortion, and the dynamical charges are very close to their formal values.¹⁷ This suggests that in YMnO_3 , similar to the BaMF_4 systems discussed in the present paper, ionic polarizability does not have any effect on the ferroelectric properties. A

subsequent analysis of the phonon modes of the corresponding centrosymmetric reference structure suggested that YMnO_3 is in fact an *improper ferroelectric*, where the ferroelectricity is due to the symmetry-allowed coupling of a stable polar zone-center phonon mode to an unstable zone-boundary mode.⁵⁸

The present study shows that such “geometric ferroelectricity” is not restricted to improper ferroelectrics, but that size effects can also directly lead to instable polar zone center phonon modes. Thus, BaNiF_4 , and with it the whole class of BaMF_4 multiferroics, represent the first confirmed example of a *proper* geometric ferroelectric.

In summary, we have presented an *ab initio* study of the structural, electronic, and magnetic properties of the multiferroic barium fluorides BaMF_4 with $M = \text{Mn, Fe, Co, and Ni}$. The ferroelectricity in these systems is due to a single unstable polar zone-center phonon. The instability is triggered solely by size effects, and no charge transfer occurs as a result of the structural distortion. In addition, we have shown that the LSDA+ U method results in a good description of the electronic structure of these systems. Our work represents the first *ab initio* demonstration of a proper geometric ferroelectric and the first such study of a non-oxide multiferroic.

Acknowledgments

This work was supported by the NSF’s *Chemical Bonding Centers* program, Grant No. CHE-0434567 and made use of the central facilities provided by the NSF-MRSEC Award No. DMR05-20415. The authors thank Craig J. Fennie and J. F. Scott for valuable discussions.

* Electronic address: ederer@mrl.ucsb.edu

¹ M. Fiebig, J. Phys. D: Appl. Phys. **38**, R123 (2005).

² N. A. Spaldin and M. Fiebig, Science **309**, 391 (2005).

³ J. Wang, J. B. Neaton, H. Zheng, V. Nagarajan, S. B. Ogale, B. Liu, D. Viehland, V. Vaithyanathan, D. G. Schlom, U. V. Waghmare, et al., Science **299**, 1719 (2003).

⁴ J. B. Neaton, C. Ederer, U. V. Waghmare, N. A. Spaldin, and K. M. Rabe, Phys. Rev. B **71**, 014113 (2005).

⁵ N. A. Hill and K. M. Rabe, Phys. Rev. B **59**, 8759 (1999).

⁶ T. Lottermoser, T. Lonkai, U. Amann, D. Hohlwein, J. Ihringer, and M. Fiebig, Nature (London) **430**, 541 (2004).

⁷ T. Kimura, T. Goto, H. Shintani, K. Ishizaka, T. Arima, and Y. Tokura, Nature (London) **426**, 55 (2003).

⁸ J. F. Scott, Rep. Prog. Phys. **12**, 1055 (1979).

⁹ H. G. v. Schnering and P. Bleckmann, Naturwissenschaften **55**, 342 (1968).

¹⁰ M. Eibschütz, H. J. Guggenheim, S. H. Wemple, I. Camlibel, and M. DiDomenico Jr., Phys. Lett. **29A**, 409 (1969).

¹¹ M. DiDomenico Jr., M. Eibschütz, H. J. Guggenheim, and I. Camlibel, Solid State Commun. **7**, 1119 (1969).

¹² E. G. Spencer, H. J. Guggenheim, and G. J. Kominiak, Appl. Phys. Lett. **17**, 300 (1970).

¹³ S. M. Shapiro, R. A. Cowley, D. E. Cox, M. Eibschütz, and H. J. Guggenheim, in *Proceedings of the Conference on Neutron Scattering, Gatlinburg, TN*, edited by R. M. Moon (1976), pp. 399–405.

¹⁴ M. Eibschütz and H. J. Guggenheim, Solid State Commun. **6**, 737 (1968).

¹⁵ N. A. Hill, J. Phys. Chem. B **104**, 6694 (2000).

¹⁶ R. Seshadri and N. A. Hill, Chem. Mater. **13**, 2892 (2001).

¹⁷ B. B. van Aken, T. T. M. Palstra, A. Filippetti, and N. A. Spaldin, Nature Materials **3**, 164 (2004).

¹⁸ C. Ederer and N. A. Spaldin, Nature Materials **3**, 849 (2004).

¹⁹ P. E. Blöchl, Phys. Rev. B **50**, 17953 (1994).

²⁰ G. Kresse and J. Furthmüller, Phys. Rev. B **54**, 11169 (1996).

²¹ G. Kresse and D. Joubert, Phys. Rev. B **59**, 1758 (1999).

²² R. O. Jones and O. Gunnarsson, Rev. Mod. Phys. **61**, 689 (1989).

²³ S. L. Dudarev, G. A. Botton, S. Y. Savrasov, C. J.

- Humphreys, and A. P. Sutton, Phys. Rev. B **57**, 1505 (1998).
- ²⁴ V. I. Anisimov, F. Aryasetiawan, and A. I. Liechtenstein, J. Phys.: Condens. Matter **9**, 767 (1997).
- ²⁵ C. Ederer and N. A. Spaldin, Phys. Rev. B **71**, 224103 (2005).
- ²⁶ R. D. King-Smith and D. Vanderbilt, Phys. Rev. B **47**, R1651 (1993).
- ²⁷ D. Vanderbilt and R. D. King-Smith, Phys. Rev. B **48**, 4442 (1993).
- ²⁸ R. Resta, Rev. Mod. Phys. **66**, 899 (1994).
- ²⁹ E. T. Keve, S. C. Abrahams, and J. L. Bernstein, J. Chem. Phys. **51**, 4928 (1969).
- ³⁰ F. Averdunk and R. Hoppe, Z. Anorg. Allg. Chem. **559**, 111 (1988).
- ³¹ E. T. Keve, S. C. Abrahams, and J. L. Bernstein, J. Chem. Phys. **53**, 3279 (1970).
- ³² M. Welsch, S. Kummer-Dörner, B. Peschel, and D. Babel, Z. Anorg. Allg. Chem. **625**, 1255 (1999).
- ³³ A. Bandyopadhyay, J. Velez, W. H. Butler, S. K. Sarker, and O. Bengone, Phys. Rev. B **69**, 174429/1 (2004).
- ³⁴ O. Bengone, M. Alouani, J. Hugel, and P. Blöchl, Computational Materials Science **24**, 192 (2002).
- ³⁵ A. B. Sushkov, O. Tchernyshyov, W. R. II, S. W. Cheong, and H. D. Drew, Phys. Rev. Lett. **94**, 137202 (2005).
- ³⁶ Z. J. Huang, Y. Cao, Y. Y. Sun, Y. Y. Xue, and C. W. Chu, Phys. Rev. B **56**, 2623 (1997).
- ³⁷ I. Solovyev, N. Hamada, and K. Terakura, Phys. Rev. B **53**, 7158 (1996).
- ³⁸ W. E. Pickett, S. C. Erwin, and E. C. Ethridge, Phys. Rev. B **58**, 1201 (1998).
- ³⁹ M. Cococcioni and S. de Gironcoli, Phys. Rev. B **71**, 035105 (2005).
- ⁴⁰ R. E. Cohen, Nature **358**, 136 (1992).
- ⁴¹ A. Filippetti and N. A. Hill, Phys. Rev. B **65**, 195120 (2002).
- ⁴² D. E. Cox, M. Eibschütz, H. J. Guggenheim, and L. Holmes, J. Appl. Phys. **41**, 943 (1970).
- ⁴³ M. Eibschütz, L. Holmes, H. J. Guggenheim, and D. E. Cox, Phys. Rev. B **6**, 2677 (1972).
- ⁴⁴ D. E. Cox, S. M. Shapiro, R. A. Cowley, M. Eibschütz, and H. J. Guggenheim, Phys. Rev. B **19**, 5754 (1979).
- ⁴⁵ E. L. Venturini and F. R. Morgenthaler, in *Conference on magnetism and magnetic materials* (1974).
- ⁴⁶ P. W. Anderson, in *Magnetism*, edited by G. T. Rado and H. Suhl (Academic Press, 1963), vol. 1, chap. 2, pp. 25–83.
- ⁴⁷ P. Baettig, C. Ederer, and N. A. Spaldin, Phys. Rev. B **72**, 214105 (2005).
- ⁴⁸ P. Novák and J. Ruzs, Phys. Rev. B **71**, 184433 (2005).
- ⁴⁹ I. V. Solovyev, Phys. Rev. B **65**, 144446 (2002).
- ⁵⁰ C. Ederer and N. A. Spaldin, cond-mat/0602400 (2006).
- ⁵¹ T. Moriya, in *Magnetism*, edited by G. T. Rado and H. Suhl (Academic Press, 1963), vol. 1, chap. 3, pp. 85–125.
- ⁵² P. Ghosez, J.-P. Michenaud, and X. Gonze, Phys. Rev. B **58**, 6224 (1998).
- ⁵³ V. M. Goldschmidt, Naturwissenschaften **14**, 477 (1926).
- ⁵⁴ P. J. Edwardson, L. L. Boyer, R. L. Newman, D. H. Fox, J. R. Hardy, J. W. Flocken, R. A. Guenther, and W. Mei, Phys. Rev. B **39**, 9738 (1989).
- ⁵⁵ R. G. Gordon and Y. S. Kim, J. Chem. Phys. **56**, 3122 (1972).
- ⁵⁶ F. Claeysens, J. M. Oliva, D. Sánchez-Portal, and N. L. Allan, Chem Commun. pp. 2440–2441 (2003).
- ⁵⁷ C.-G. Duan, W. N. Mei, J. Liu, W.-G. Yin, J. R. Hardy, R. W. Smith, M. J. Mehl, and L. L. Boyer, Phys. Rev. B **69**, 033102 (2004).
- ⁵⁸ C. J. Fennie and K. M. Rabe, Phys. Rev. B **72**, 100103(R) (2005).
- ⁵⁹ C. J. Bradley and A. P. Cracknell, *The mathematical theory of symmetry in solids* (Oxford University Press, 1972).
- ⁶⁰ In many papers this space group is denoted as $A2_1am$, referring to an alternative setting for the base-centered orthorhombic lattice vectors. Here, we use the notation of Ref. 59.